Insights on the Cenozoic climatic history of Southeast Australia from kaolinite dating

Maximilien Mathian, Mathieu Chassé, Georges Calas, William L Griffin, Suzanne Y O'Reilly, Thibault Buisson, Thierry Allard

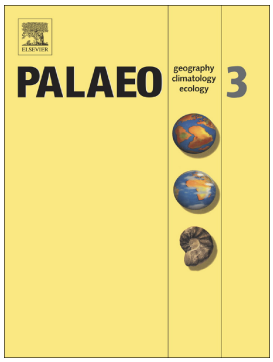

Insights on the Cenozoic climatic history of Southeast Australia from kaolinite dating

Maximilien Mathian, Mathieu Chassé, Georges Calas, William L. Griffin, Suzanne Y. O'Reilly, T. Buisson, Thierry Allard

PII: S0031-0182(22)00382-0

DOI: https://doi.org/10.1016/j.palaeo.2022.111212

Reference: PALAEO 111212

To appear in: *Palaeogeography, Palaeoclimatology, Palaeoecology*

Received date: 30 October 2021

Revised date: 31 July 2022

Accepted date: 21 August 2022

Please cite this article as: M. Mathian, M. Chassé, G. Calas, et al., Insights on the Cenozoic climatic history of Southeast Australia from kaolinite dating, *Palaeogeography, Palaeoclimatology, Palaeoecology* (2022), https://doi.org/10.1016/j.palaeo.2022.111212

Insights on the Cenozoic climatic history of southeast Australia from kaolinite dating

Maximilien Mathian[1,2*], Mathieu Chassé[1], Georges Calas[1], William L. Griffin[3], Suzanne Y. O'Reilly[3], T. Buisson[1], Thierry Allard[1]

[1]*Sorbonne Université, Institut de minéralogie, de physique des matériaux et de cosmochimie, UMR CNRS 7590, IRD, MNHN, F-75005 Paris, France*
[2]Université Paris-Saclay, Géosciences Paris-Saclay GEOPS, UMR CNRS 8148, Orsay, France
[3]*ARC Centre of Excellence for Core to Crust Fluid Systems (CCFS) and GEMOC, Department of Earth and Environmental Sciences, Macquarie University, NSW 2109, Australia*
**corresponding author:* maximilien.mathian@gmail.com

Abstract

Australia hosts some of Earth's oldest regolith. They were preserved through geological time thanks to exceptionally low erosion rates affecting large parts of this continent. Accurate chronological constraints about their formation and evolution are abundant in its northern and western regions, but they remain underexplored in its southern and eastern parts, limiting the determination of the extent and impact of Cenozoic paleoclimatic events over this continent. To address this question, we provide a new set of chronological data obtained from a tropical regolith from southeastern Australia close to the western side of the Australian Great Escarpment (Syerston–Flemington, New South Wales). The Syerston regolith, known for its anomalous Sc content, exhibits a thick duricrust (18 m deep) comprising both an *in situ* and a detrital component. The thickness of these indurated horizons, and particularly the presence of the detrital duricrust protecting the profile from secondary vertical weathering of low intensity and erosion, were favourable conditions for the conservation of a long-term record of local paleoweathering history. Electron Paramagnetic Resonance (EPR) dating of phyllosilicates allows the discrimination of two generations of kaolinite formed at 10.1 ±2.3 Ma and 3.8 ± 0.9 Ma, trapped within the *in situ* duricrust. In parallel, the detrital horizon hosts phyllosilicates with an age of 8.2 ± 2.8 Ma and 1 ± 0.3 Ma close to its top. Such ages confirm the hypothesis that, following the end of tropical Middle Miocene period, the Late Miocene climate in southeast Australia was still favorable to the development of tropical weathering covers. These results, combined with other dating studies from the literature, suggest that a large part of the extended coastal regions of Australia suffered a warm and wet climate from the Mid-Miocene to the beginning of Late Miocene. However, this hypothesis, as well as the extent of hot and wet climate over Central Australia during the Late-Miocene, period of the onset of the Australian aridity, still need to be constrained by complementary paleoregolith dating studies.

Keywords: *southeastern Australian Regolith, Laterite, EPR-Dating of phyllosilicates, Kaolinite, Mineralogy*

1. Introduction

Preserved ancient regoliths are invaluable archives of the evolution of continental surfaces (Vasconcelos et al., 1994 ; Beauvais et al., 2016; Mathian et al., 2019; Vasconcelos et al., 2019). Mineral dating of weathering covers, a field of study initially explored by e.g. Bird et al. (1990), Ambrosi and Chen (1990) and Alpers and Brimhall (1988), is able to provide chronological constraints about their formation as well as information on the climatic, geomorphological, hydrological and tectonic factors that have affected their geochemical dynamics through the geological times (Retallack, 2010; Mathian et al., 2020). Among all continents, Australia is unique regarding the stability of its regolith (Vasconcelos et al., 2008). Indeed, relics of ancient landscapes inherited from the Precambrian to the Cenozoic are preserved (e.g. Schmidt and Williams, 2017) due to unusual erosion rates, commonly lower than 6 m/Ma (Gale, 1992; Biermann and Caffee, 2002; Vasconcelos et al., 2008). To complement the usual paleontological record and paleoclimatic proxies, the local regolith profiles are thus a key to highlight and/or constrain spatially and temporally the succession of climatic events that affected the parts of the Australian continent considered in this study (e.g. Metzger and Retallack, 2010).

The chronology governing the formation and evolution of the Australian regolith since the end of the Mesozoic is well constrained in Northern and Western Australia (e.g. Vasconcelos, 2008; Fig. 1) thanks to K/Ar or Ar/Ar dating of Mn-oxides (Vasconcelos, 1999), (U-Th)/He dating of Fe-oxides (Shuster et al., 2005) and paleomagnetic studies (e.g. Butler, 1992). Some evidence of Late Cretaceous/early Cenozoic regoliths (*ca* 65 to 55 Ma, Vasconcelos et al., 2008; Miller et al., 2017) are found in northern Australia, and are often correlated with high elevation topographic surfaces. However, most of the literature on laterite dating describes weathering profiles that host secondary minerals that crystallized during the Miocene (23 to 5.3 Ma) and Quaternary (2.5 Ma to the present; Dammer et al., 1996, Vasconcelos, 1998; Li and Vasconcelos, 2002; Vasconcelos et Conroy, 2003; Pidgeon et al., 2004; Pillans, 2004 and references therein; Heim et al., 2006; Feng and Vasconcelos, 2007; Vasconcelos et al., 2008; Wells et al., 2019). It clearly demonstrates the prevalence of a hot and wet climate in this period over Northern and Western Australia. In addition, the Late Eocene/Oligocene (*ca* 40-30 Ma) transitional climate (e.g. global cooling, see Korasidis et al., 2019) inferred for northwestern Australia, indicates the initial establishment of a fluviatile system, whose traces are preserved today in the form of paleochannels (CID, Ramanaidou et al., 2003) filled with reworked duricrust clasts and called channel iron deposits (Heim et al., 2006; Vasconcelos et al., 2013; Miller et al., 2017). (U-Th)/He dating studies demonstrated that the warm and wet Miocene climate, and to a lesser extent the Early Pliocene tropical climate (Quilty, 1994; McLaren et al., 2014), were the most favorable to the formation and induration of these CID and probably to the development of tropical regoliths in northern and western Australia (Heim et al., 2006; Morris et al., 2007; Danisik et al., 2013; Vasconcelos et al., 2013; Ramanaidou et al., 2017; Miller et al., 2017). However, only stratigraphic evidence suggests a Miocene origin for laterite covers and kaolin deposits from southeast and central Australia (Pickett, 2003, Metzger and Retallack, 2010). The precise timing of formation and evolution of tropical regolith profiles in

southeast Australia is lacking (Fig. 1), contributing to the controversy about the extent of the Mid-Miocene Climatic Optimum wet and warm climate over the Australian continent (Travouillon et al., 2009; Metzger and Retallack, 2010; Herold et al., 2011; Greenwood et al., 2012; McLaren et al., 2014).

This study aims to provide new chronological constraints on the formation and evolution of weathering covers in southeastern Australia and to evaluate the local link between fine-scale mineralogical variations and climate forcing in the light of previous studies in tropical environments (Girard et al., 2002; Retallack, 2010; Bonnet et al., 2016; Mathian et al., 2019, Putzolu et al., 2020). It is focused on a lateritic profile (Syerston–Flemington, New South Wales) developed over an ultramafic complex west of the Great Dividing Range, a region preserved from intense erosion since at least the Mid-Mesozoic period (Vasconcelos et al., 2008). This laterite is of high interest due to its structure and inferred formation process, as an *in situ* profile is covered by a thick detrital duricrust (11 m deep). Indeed, previous dating studies (Mathian et al., 2019, 2020; Allard et al., 2020) demonstrated that in uncapped regoliths, rejuvenation processes of secondary minerals triggered by the Quaternary precipitations results in the presence of minerals with a Quaternary age that can, with time, mask the signal of older minerals. Such a phenomenon is also observed within exposed duricrusts that often host rejuvenated iron oxides and oxyhydroxides (Allard et al., 2018; Wells et al., 2019; Albuquerque et al. 2020). Accordingly, the detrital duricrust covering the *in situ* one in Syerston's regolith is expected to have favoured the preservation of a more robust long-term record of paleoweathering history that could be obliterated in uncapped regoliths from the inter-tropical zones. Here we use Electron Paramagnetic Resonance (EPR), also called Electron Spin Resonance (ESR), dating of kaolinite (Balan et al., 2005) on areas enriched kaolinite from both duricrust sections (*in situ* and detrital) of this profile. This dating method is currently not commonly used in the literature, but previous findings confirmed that the EPR dating applied to Cenozoic kaolinites provides consistent results. For instance, in tropical regoliths, there is a good correlation between kaolinite ages and periods identified as affected by strong precipitation (Mathian et al., 2019; 2020). Kaolinite trapped within ferruginous duricrusts also, predictably, exhibits slightly higher ages than the associated iron oxides dated by (U-Th)/He. Accordingly, the kaolinite ages obtained from the Syerston profile, combined with the geochemical and morphological characteristics of the dated phyllosilicates, allow discrimination of three main periods of kaolinite formation and help to decipher the timing of formation and evolution dynamics of southeastern Australian regolith.

2. Geological context of the lateritic regolith

The studied lateritic profile (Fig. 1, Fig. 2) is developed over the Tout mafic–ultramafic complex (*ca* 440 Ma). This geological formation belongs to the Goonumbla–Trangie Volcanic Belt, a part of the larger Tasman fold belt system (e.g. Fergusson et al., 2009; Aitchsion and Buckman, 2012). This volcanic belt resulted from successive episodes of continental breakup and accretion since the Precambrian. Particularly, the Tout complex formed during a shoshonitic

magmatic event occurring ca 440 Ma ago. This elliptical intrusion (16 km x 6.5 km) is an Alaskan-type complex that intruded within the regional metamorphosed quartz-rich turbidites of the Girilambone group. The Tout complex displays a concentric succession of lithotypes with serpentinite and dunite at the center of the complex, surrounded by pyroxenite and a monzonite-rich area (Fig. 2C). By studying regoliths developed over the sediments from the Girilambone group, Chan et al. (2009) suggested that these sediments, and likely the Tout complex, were exposed to weathering due to a progressive erosion that begun during the Late Cretaceous. The exposure of the Tout complex to precipitations should post-date this period and is likely the cause of development of its thick regolith (*ca* 25/30 m). This laterite hosts the world-class Syerston–Flemington scandium deposit (Chassé et al., 2019). Placers and regoliths in the area, associated with Alaskan-type complexes, are also commonly enriched in platinum-group elements as well as Ni and Co (Andrew et al., 1995). The local regolith is located on a topographic high of 315 m above sea level, relict from a dissected scarp perpendicular to the Great Dividing Range (Fig. 2A,B). This passive margin is characterised by two distinct erosion regimes in its two flanks. The eastern side of the escarpment suffered high erosion rates reaching 53 ± 3 m /Ma (Heimsath et al., 2001), however the landscapes located west of its flank have not undergone intense erosion since the Early Mesozoic (Vasconcelos et al., 2008 and references therein). The present-day Syerston–Flemington region is a warm grassland, with summer drought, an average temperature of *ca* 17.5 °C and annual precipitations of ca 532 mm/yr.

Despite the present-day climate that cannot promote the formation of a tropical regolith, the local regolith follows the organization of a lateritic profile developed over ultramafic rocks (Fig. 3, Supplementary Information (SI) 1; Chassé et al., 2017; 2019) similar to the one described by Aleva and Creutzberg (1994). This preserved laterite can be divided into: 1) a saprolite (saprock, saprolite and plasmic zone) rich in Mg/Fe-smectite and pyroxene inherited from the local primary rock; 2) a mottled zone, about 3 m thick, including smectite-rich mottles dispersed within an iron (oxyhydr)oxides-rich matrix but also containing traces of quartz, kaolinite, Mn oxides and authigenic calcite; 3) an *in situ* duricrust (*ca* 7 m thick) dominated by hematite and goethite, enriched in kaolinite and with high Sc concentrations at its base (Chassé et al., 2019) but also richer in gibbsite in its top pisolith-rich levels; 4) a detrital duricrust, about 11 m thick, composed of Fe pisoliths, lateritic clasts and rarer quartz grains indurated by a matrix of iron (oxyhydr)oxides and gibbsite that can also contain kaolinite (Fig. 3, SI 1 and 2). The top of this weathering profile suffered erosional processes forming a 0.3 m thick lateritic gravel horizon mixed with soil material richer in organic matter. The development of the detrital duricrust over the local regolith should have promoted the preservation of a long-term record of paleoweathering history that may be lost in uncapped loose regoliths.

3. Material and Methods

3.1 Geochemical and mineralogical analyses

For this dating study, four samples were selected, based on their high kaolinite contents (Fig. 3; Chassé et al., 2019) and the readability of their EPR spectra, particularly of the spectral region hosting kaolinite radiation-induced defects (RID), used for their dating (Fig. 3, see section 4.2 below). Two samples from the *in situ* duricrust, insitu1 and insitu2, came from 16.4 m and 16 m deep respectively (Fig. 3, SI 2A). In the detrital duricrust, two samples were also selected at depths of 6.5 m and 3 m (samples detrit1 and detrit2, respectively). All the samples were air-dried at room temperature.

Bulk chemical analyses were performed by X-ray fluorescence (XRF) on finely crushed powders (< 50 µm), obtained using a tungsten carbide mill for major elements and by ICPMS analyses following the protocol of Chassé (2017) and Chassé et al. (2019). The mineralogy of the profile given in this article came from the results published by Chassé et al. (2019). It was determined by X-ray diffraction combined with Rietveld refinement on ca 30 g of chip samples collected at specific depths along the laterite drill core (see Chassé et al., 2019 for more information).

The nanoscale organization of the selected samples and the morphology of kaolinite grains were observed using a Gemini Zeiss Ultra 55 Field Emission Gun (FEG) Scanning Electron Microscope (SEM) used at a working distance of 7.5 mm and an energy of 15 kV. SEM observations were made in secondary electron mode for morphological investigations.

The remaining selected samples were crushed. Iron oxides were leached following the dithionite-citrate-bicarbonate (DCB) protocol of Mehra and Jackson (1960). Due to the high iron-oxide concentration, an average of ten successive treatments was performed on each sample. The clay fractions (< 2 µm) of the four samples were then recovered by sedimentation.

The clay fraction was investigated by Fourier Transform Mid-infrared spectroscopy (FTIR) with a Nicolet Magna 560 FTIR spectrometer. Pellets were obtained by mixing 1 mg of each sample and 150 mg of KBr. The spectral resolution was 2 cm^{-1} in the 400-4000 cm^{-1} range by averaging 100 scans.

3.2 Electron paramagnetic resonance dating procedure

EPR spectra were obtained by analyzing the clay fraction of each samples using a Bruker EMXplus™ spectrometer equipped with a high-sensitivity cavity used at X-Band (9.44 GHz). Acquisitions were performed with a magnetic field modulation frequency of 100 kHz and a microwave power of 40 mW. An amplitude of magnetic field modulation of 0.3 mT at 110 K was used to record zoomed spectra on the RID spectral region of EPR spectra (Fig. 4) and 0.5 mT at ambient temperature was used for total spectrum acquisition (Fig. 4). Samples were measured in calibrated silica tubes (Suprasil grade) and the obtained spectra were normalized using the volume of the sample and its position in the spectrometer cavity. Note that the DCB treatments, used on bulk samples, leave kaolinite minerals untouched, preserving the RID EPR signal of kaolinite samples (Angel and Jones, 1974).

Alpha irradiations were performed on the clay fraction of the four samples (see SI 3A) using a 1.5 MeV He^+ ion beam with a 0.3 A current in the ARAMIS electrostatic accelerator (Orsay, France). The range of 1.5 MeV He^+ ions in kaolinite, as calculated by the SRIM code (Ziegler et al., 2010), is 4 µm. This value defines the thickness of the 30 mg kaolinite samples deposited on steel plates for accelerator irradiation. In total, six different ion beam fluences ($3 \cdot 10^{11}$, $6 \cdot 10^{11}$, 10^{12}, $3 \cdot 10^{12}$, $6 \cdot 10^{12}$ and 10^{13} ions $\cdot$ cm^{-2}), producing respectively irradiation doses from 70 to 2342 kGy, were used to irradiate aliquots from each dated kaolinite sample (SI 3A).

Polished sections of resin-embedded samples were prepared to map the distribution of uranium and correct the dose rates using the induced Fission-tracks methodology. Thin sections were covered by a Kapton® foil as external detector (Kleeman and Lovering, 1967) and irradiated by thermal neutrons, at the FRM2 reactor in Munich (Germany) during 600 s using an instant flux of $1.15 \cdot 10^{13}$ neutrons $\cdot$ cm^{-2} $\cdot$ s. Standard glasses (i.e. SRM-613 from the National Institute of Standards and Technology) were also covered by Kapton® foil and irradiated for the calibration of the U content (12.33 µg/ g of normalized U for the SRM-613). Fission tracks registered in the Kapton® foils were revealed by etching for 8 minutes in an aqueous solution of 14 % NaClO and 12 % NaCl heated at 100 °C (Sélo, 1983). Fission tracks were counted optically using an optical microscope with a 1000 times magnification.

4. Results

4.1 Mineralogy and crystal-chemistry of kaolinite from the Syerston—Flemington regolith

The Syerston regolith is characterized by horizons with a distinct mineralogical and spatial organization (Fig. 3; SI 1; SI 2A; Chassé et al., 2017; 2019). Kaolinite form within the mottled zone at the expense of smectite, a phenomenon common in tropical regoliths developed over ultrabasic rocks (Colin et al., 1990; Yongue-Fouateu et al., 2009). It becomes a dominant phase at the base of the *in situ* duricrust but decreases in its upper part in parallel with the increase of gibbsite content (Fig. 3; SI 2). In the detrital duricrust, it remains abundant (up to 38%, SI 2A,B), particularly in samples rich in laterite clasts (Chassé et al., 2019).

Both the morphology and crystal-chemistry of kaolinite from the four selected samples were investigated using SEM analyses combined with FTIR and EPR spectroscopies. The insitu1 sample has a structure characterized by a low porosity, often filled with kaolinite. In this sample, kaolinite is morphologically homogeneous, characterized by micrometric platelets mixed with submicrometric iron (oxyhydr)oxides that often crystallized at the surface of kaolinite (SI 4A,B). The organisation of the insitu2 sample is similar with a higher porosity. Kaolinite also displays thicker platy sections. They are, scarcely, found grouped as vermicular-like structures (Fig. 5A). By contrast, the matrix of detrit1 sample is dominated by iron (oxyhydr)oxides (SI 2A). Kaolinite shows two distinct forms, geometric, thick (*ca* 200 to 400 nm) sections more or less rounded (Fig.

5B, SI 4 C,D,E) or small vermicules (<5 µm) displaying cracks and secondary overgrowths (Fig. 5B). In addition to kaolinite crystals, small rods (<5 µm) with a kaolinite-like composition suggest minor detrital halloysite (Fig. 5B, SI 4C) probably coming from the erosion of the surrounding sedimentary formations (see Fig. 2C). The detrit2 sample is dominated by a bulk matrix with kaolinite, gibbsite, iron oxides and oxyhydroxides. Kaolinite vermicules are divided into large and well-preserved ones with a 1-10 µm in size (Fig. 5C), and minor vermicules exhibiting small size, cracks and overgrowths similar to the ones from the detrit1 sample. Halloysite rods are not observed in this last sample.

The OH-stretching band region of the FTIR spectra provides information on the structural disorder of kaolinite (Farmer, 1974; Russell and Fraser, 1994; Balan et al., 2007). The FTIR spectra of detrit2, insitu1 and insitu2, display a similar signal, with broad and weak bands at 3670 and 3652 cm^{-1}, pointing to a disordered kaolinite (Fig. 5D). The insitu2 sample also display a weak and broad absorption at 3600 cm^{-1} band, characteristic of Fe^{3+} substitution in the kaolinite structure. The detrit1 sample, which also contained gibbsite and halloysite, that potentially impact the OH stretching bands of kaolinite, is characterized by 3670 and 3652 cm^{-1} bands less defined than in the other samples, in agreement with the presence of disordered kaolinite and halloysite. The increase of the $Fe^{3+}_{(I)}$ signal of its EPR spectra (Fig. 5F), compared to the other spectra, confirms that this kaolinite is more disordered than kaolinites from the other samples (Balan et al., 1999; 2007; Gaite et al., 1997).

4.2 Dating of kaolinite: from the radiation induced defects to kaolinite ages

4.2.1 Determination of Paleodoses

In the studied regolith, the EPR signal of radiation-induced defects has a weak amplitude for all kaolinites (SI 3B) with variations ranging between 1.24 ± 0.18 a.u. and 6.33 ± 0.9 a.u. (Table 1). It might indicate either a weak radiation background or a young age of crystallization of the kaolinite. After the irradiation procedure, the determined paleodoses obtained from the modelling of the dosimetry curves (see SI 3, 5) range within one order of magnitude, i.e. from 8.1 ±1.8 kGy to 68.6 ± 22.9 kGy (Table 1).

4.2.2 Determination of the dose rates

The evolution of U and Th contents (Table 1; Chassé et al., 2019) within the studied profile shows a clear disparity between the concentration of these elements within the *in situ* duricrust (U < 1.4 ppm and Th < 7 ppm) and within the detrital duricrust, which is by comparison enriched in both U (1.3 ppm < U < 2 ppm) and Th (7 ppm < Th < 12 ppm). The resulting Th/U ratios are higher within the detrital duricrust than in the *in situ* duricrust (SI 2C). The uncorrected dose rates of lateritic samples can be calculated (Aitken, 1985) from present-day U, Th and K concentrations

(Table 1), but corrections must be performed for (i) the disequilibrium of the decay chains, (ii) the impact on the heterogeneous distribution of U at microscopic scale, (iii) the water content (SI3C). *(i) Soils are open systems*, which commonly show an isotopic disequilibrium of decay chains (Dequincey et al., 2002), but decay chains close to equilibrium can also be preserved (Balan et al., 2005; Mathian et al., 2020). Among daughter elements, radon is a major source of disequilibrium (SI3C). Its loss is often driven by the organisation of the sample linked to its mineralogical composition but also to other parameters like its water content (Sakoda et al., 2011). As duricrusts often have similar bulk mineralogy and a low water saturation, and as the connected porosity of the studied duricrust is low, we used a reference value of 3 % Rn loss measured in indurated lateritic materials (Sakoda et al., 2011). Such a similar approach has proven to be consistent in previous EPR dating study (Mathian et al., 2019).

(ii) Alpha radiation has a mean free path limited to 20 µm in silicates (Allard et al. 1994). Consequently, the U fraction contained within large U-bearing minerals (e.g. zircons or Ti oxides for instance) will not irradiate kaolinite from the bulk sample (e.g. Balan et al., 2005; Allard et al., 2018; Mathian et al. 2019). The U proportion contained within U-bearing minerals is estimated by mapping induced fission tracks. Due to the distinct differences in the concentration of U and Th between the *in situ* and detrital duricrust, two thin sections representative of the detrital and *in situ* duricrust were analysed. The counting of fission tracks resulting from the irradiation of thin sections demonstrates that U-bearing minerals account for 68 % of the total U in the detrital duricrust and only 10 % in the *in situ* duricrust (SI 6). Due to the scarcity of U-bearing minerals in both samples, demonstrated by the low number of fission tracks urchin (e.g. accumulation of numerous fission tracks in the same small area) on both Kapton® foils, the dose-rate impacting the kaolinite from the 20 micrometers thick rims around these minerals was neglected for the dose rate calculation (SI3C).

(iii) The soil water content can also impact the dose rate in water-saturated soils (Aitken, 1985; Mathian et al, 2020). However, long-term water saturation is limited to the mottled zone and to the saprolite, all below the studied duricrust levels (Fig. 2). Duricrusts are far beyond this saturation level due to their position. Besides, the local present-day climate and geomorphologic location also make water saturation of this duricrust unlikely. We thus raised the hypothesis that its impact on the sample dose rate since kaolinite crystallization is negligible. Resulting corrected dose rates vary over one order of magnitude between the *in situ* laterite (insitu1: 1.53 ± 0.15 Gy/ka ; insitu2: 2.12 ± 0.16 Gy/ka), and the detrital laterite (detrit1: 8.4 ± 0.57 Gy/ka ; detrit2: 10.26 ± 0.68 Gy/ka, Table 1). A large part of the alpha irradiation (68% of U contained in U-bearing minerals) is not experienced by the kaolinites within the detrital samples but the high U and Th contents in the detrital duricrust compared with the *in situ* duricrust explain these contrasting dose rates. Complimentary corrected dose rates calculated using less likely hypotheses in the Syerston regolith context (e.g.: Rn loss of 40% or 100%, a water content of 10%, progressive accumulation of mobile U, SI3C) give values of the same order of magnitude, except when considering an improbable extreme case with 100% Rn loss.

4.2.3 Calculation of the Kaolinite ages

The calculated ages range from 1± 0.3 Ma to 10.1 ± 2.3 Ma (Table 1, Fig. 6). The detrit2 sample, the richest in kaolinite, has the youngest age (1 Ma), while the sample closer to the base of the detrital duricrust, detrit1, has a Miocene age (here estimated at 8 Ma, see SI 3B). The ages from the *in situ* duricrust are also different (Table 1, Fig. 6): the insitu1 sample has also a Miocene age (ca 10 Ma), while the insitu2 is of Pliocene age (ca 4 Ma). Regardless of the hypotheses used to calculate these ages (SI3), EPR dating results highlight three main periods of kaolinite crystallization of the Syerston's kaolinites: Quaternary, Pliocene and Late/Middle Miocene.

5. Discussion

5.1 Formation and evolution of the Syerston—Flemington regolith

Dating kaolinite from the Syerston regolith reveals that at least three distinct generations of kaolinites are present within this duricrust, as observed within tropical regoliths from India (Mathian et al., 2019) and Amazonia (Balan et al., 2005). It supports the concept of an episodic evolution of the mineralogy of tropical regoliths that could possibly occur worldwide. In the studied regolith, kaolinites with Miocene ages are found both at the bases of both the *in situ* and the detrital duricrust. Younger ages are found closer to the tops of these two horizons (Fig. 6). Such observations, combined with the variation of kaolinite morphologies between the *in situ* and detrital duricrust indicate distinct formation and evolution processes for these two levels (SI 7).

5.1.1. Timing of in situ *duricrust formation and evolution*

The insitu1 sample is located 40 cm below the insitu2 sample and is older (Late/Middle Miocene versus Pliocene, Fig. 6). Insitu2 kaolinite crystals are thicker and better-ordered according to SEM observations, an analysis confirmed by the shape of its FTIR spectra. In addition, and contrary to Insitu1, Insitu2 displays a FTIR absorption band at 3600 cm^{-1}, characterizing Al^{3+}/Fe^{3+} substitution in its kaolinite structure (Fig. 5). These differences between the characteristics of the insitu1 and insitu2 kaolinites indicate that they crystallized within distinct geochemical microenvironments (Tardy et al., 1993; Mathian et al., 2019) leading to distinctive kinetics of crystallization. Such variation between kaolinite from two closely-spaced samples can be explained by the protection of the insitu1 kaolinite from dissolution/recrystallization processes (see SI 7) following their Miocene crystallization, due to the low porosity of this sample. Comparison of their two Th/U ratios supports this idea (Table 1). As thorium is less mobile than U, the Th/U ratio in duricrusts increases with successive mineral dissolution/recrystallization processes (Monteiro et al., 2014). The higher Th/U ratio in the insitu2 sample supports the assumption that it underwent more episodes of transformation of its constituent phases, including kaolinite. By considering the validity of the hypotheses used for the ages calculations, these results

suggest that the Syerston regolith started to develop a duricrust horizon prior to 10 Ma ago, or at least during the Late/Middle Miocene considering the less likely hypotheses described in SI3C. Indeed, kaolinite generally forms in the lateritic horizons over ultramafic primary-rocks at the expanse of a first generation of phyllosilicate, here smectite, which constitutes the saprolite. Nevertheless, kaolinite from the top section of this *in situ* duricrust suffered at least one rejuvenation process during the Pliocene.

5.1.2. Detrital duricrust formation and evolution: a memory of landscape erosion

The detrital duricrust (11 m thick in the present-day, Fig. 6) hosts kaolinite with a Miocene age at its base (*ca* 8 Ma considering the chosen EPR dating hypotheses) but also Quaternary kaolinite near to the top of the profile. The presence of halloysite rods (Fig. 5), visible only with the SEM, the high content of U and Th, with U essentially contained within (probably detrital) U-bearing minerals (Table 1) and the presence of quartz clasts (SI 2A), all point to the fact that a part of the detrital material came from the surrounding weathered sedimentary rocks of the Girilambone group (Fig. 2C). Kaolinite from the insitu1 sample is fractured or occurs as partially dislocated kaolinite vermicules and more or less rounded geometric platy sections (Fig. 5, SI 4) indicating their detrital origin. They are inferred to have eroded from surrounding laterites that developed during the Miocene in the Syerston landscape. As the EPR dating of kaolinite provides an average crystallization age of the kaolinite present in a sample, the presence of kaolinite overgrowths (Fig. 5) may be a possible cause of the observed shift of age between 10 Ma for the insitu1 sample and the age of 8 Ma calculated in this detrital horizon. The low content of halloysite may also contribute to this shift. The Quaternary kaolinites detected in one sample are also characterized by a high Th/U ratio (Table 1) and show two types of kaolinite morphologies: small cracked and dislocated vermicules of kaolinite as well as numerous large and preserved vermicules of kaolinite (Fig. 5). These latter younger kaolinites formed at the expense of older kaolinite from the detrital duricrust due to at least one episode of dissolution/recrystallization during the Quaternary, estimated at *ca* 1 Ma.

The observed Miocene detrital kaolinites, slightly rejuvenated, confirmed that the Late/Middle Miocene was characterized by a tropical climate promoting the formation of weathering covers in the Syerston region. The age of induration of the detrital duricrust should be comprised between the Pliocene (*ca* 4 Ma considering the chosen EPR dating hypotheses, rejuvenation of the top of the *in situ* duricrust) and the Quaternary (*ca* 1 Ma, rejuvenation of the top of the detrital duricrust). Rejuvenation of the top of the *in situ* duricrust through water percolation must indeed be limited to immediate surrounding fractures considering the capping by 11 m of an indurated detrital duricrust with a globally low connected porosity.

5.1.3. Inferences on erosion regime in the Syerston's region

The erosion regime affecting this dissected scarp west of the Australian Great Dividing Range can be approximately constrained by the obtained kaolinite ages. The regolith altitude is 315 m and it is capped by a thick detrital duricrust with maximum Pliocene age (*ca* 4 Ma). Detrital duricrusts form from the induration of clasts accumulated in a depositional site located at a lower elevation than the one of their initial sources (Anand et al., 2001). The current position of the regolith, on a local maximum elevation, must then be the result of the dissection of the surrounding original landscape, that should have caused the retreat of the higher elevation source area since the last 4 Ma (SI 8). The Syerston area should have been preserved from these erosional processes due to the induration of the upper part of its regolith. Nevertheless, scarp retreat of several kilometers (SI 8) should imply erosion rates higher than the 6 m/Ma observed in Central Australia (Gale et al., 1992). However, erosion rates as high as the ones from the eastern side of the Great Dividing Range (53 m/Ma, Heimsath et al., 2000; 2001) are unlikely to be due to the good preservation of the detrital duricrust, which displays only a thin horizon of dismantled duricrust (SI 1).

5.2 Paleoclimatic constraints and Syerston laterite kaolinite ages

We recognize three major periods of kaolinite crystallization in the Syerston regolith: the Late/Middle Miocene, Pliocene and Early Pleistocene (Fig. 6, Fig. 7). A Late/Middle Miocene age for tropical regoliths from this region is consistent with the non-absolute stratigraphic ages from other regoliths/kaolin deposits from New South Wales (Middle Miocene and "Post" Middle Miocene; Hunt et al., 1977; Nott et al., 1991; Picket, 2003; Metzger and Retallack, 2010). It confirms the influence of a hot and wet climate over southeast Australia during this period following a globally temperate but wet Oligocene epoch (McLaren et al., 2014). It is also consistent with paleontological evidence of the presence of a Mid-Miocene subtropical rainforest in New South Wales and of warm oceanic water close to the southeastern Australian coasts, as demonstrated by the presence of tropical foraminifera typical of this period (Fig. 7, McLaren et al., 2014, Gallagher et al., 2001). However, during the Late Miocene, the paleontological records highlight a progressive aridification that combined with decreased temperatures in eastern Australia (Gallagher et al., 2001; McLarren et al., 2014). This points to the fact that the Syerston regolith is one of the last products of the Miocene hot and wet climate from New South Wales. Such climatic condition changes could be favourable to initiate the partial dismantling of the tropical regoliths in the Syerston area and promote the accumulation of tropical regolith clasts over the dated *in situ* regolith.

The Miocene period seems to be characterized by a warm and wet climate at a global scale favoring the development of lateritic regoliths in South America (Alpers et Brimhall, 1988; Carmo et al., 2004; Balan et al., 2005; Carmo et al., 2006; Vaconcelos et al., 2015; Allard et al. 2018; Mathian et al., 2020; dos Santos Albuquerque et al., 2020; Heller et al., 2022), Africa (Beauvais et al., 2008), India (Bonnet et al., 2016; Mathian et al., 2019) and even southern China (Li et al., 2007). However, despite extensive chronological studies in western and northern Australia, the extent of this hot and wet climate characterizing the Mid-Miocene Climatic Optimum over

Australia is controversial (Travouillon et al., 2009; Metzger and Retallack, 2010; Herold et al., 2011; Greenwood et al., 2012; McLaren et al., 2014; Mao and Retallack, 2019). The kaolinite ages obtained in this study can be compared to ages obtained by Ar/Ar and K/Ar dating of tropical supergene Mn oxides and (U-Th)/He dating of iron oxides from tropical regoliths and channel iron deposits (formed under a hot and wet climate, see Heim et al., 2006). Despite the low number of studied samples, it demonstrates that the formation of tropical weathering surfaces is recorded during the Mid-Miocene but also in the beginning of Late-Miocene time in the northwest and northeast of Australia (Fig. 8). The presence of similar relics of tropical regoliths across other parts of Australia, and particularly across the whole Central Australia during this period remains a subject of debate. Indeed, large formations of tropical regoliths, dated with paleontological proxies to the Middle Miocene, are observed in the northern area of Central Australia, up to the locality of Alcoota (Central Australia, Mao and Retallack, 2019). However, paleosols from Early and Late Miocene indicate more arid conditions in other parts of Central Australia (Metzger and Retallack, 2010; Mao and Retallack, 2019). Accordingly, some authors considered that Central Australia did not suffer a wet and warm climate during the Miocene except during the Mid-Miocene Climatic Optimum wet spike, that promoted the extension of the rainforests as well as laterite development in this part of the continent. Such hypothesis cannot be confirmed by our dataset. However, the Late Miocene kaolinite ages (*ca* 10 Ma) obtained in Syerston could suggest that Southeastern Australia climate aridification was not concurrent with the one of Central Australia, but occurred closer to the end of the Miocene. As it stands, the ages of tropical regoliths recorded in the literature from the northwest, northeast Queensland and Northern Territories regions of Australia (Fig. 8) combined with our own dataset, could suggest that from the Middle to the beginning of Late Miocene, some of the extended coastal regions the Australian continent suffered a hot and wet climate, even while Central Australia began its aridification (Mao and Retallack, 2019). The spatial and temporal extent of climates favorable for laterite formation during this regional aridification needs to be determined by further dating of tropical regoliths across Australia.

The Pliocene period in southeast Australia was characterized by another episode of wet and hot climate, as demonstrated by the analysis of local paleontological proxies (Fig. 7; McGowran and Li, 1998; Gallagher et al., 2003; McLaren et al., 2014). The rejuvenation of the top of the *in situ* duricrust is probably correlated with these favourable climatic conditions. Such correlation between periods of increased precipitation and the crystallization of new generations of kaolinite within a tropical regolith is also documented in deep Indian laterite (Mathian et al., 2019). Dissolution/recrystallisation of secondary minerals is promoted in tropical regoliths through the induced changes in the water regime, that could be particularly short in time but still induced an important water circulation, as observed in Amazonia (Guinoiseau et al., 2021). It may also correspond to a climate with a water circulation sufficient to initiate the induration of the clasts constituting the local detrital duricrust. In parallel, Quaternary kaolinite formation at the top of the detrital duricrust could be the result of the continuous rejuvenation of older kaolinites due to the percolation of meteoritic waters in the top profile, a rejuvenation often observed when analysing

phyllosilicates ages in million-years old laterites. However, Quaternary tropical climate of northeastern Australia has caused the formation of recent supergene tropical deposits (Feng et al., 2001; Feng et al., 2007). Such tropical weathering pulse is also confirmed in the Southeast Queensland paleontological and marine records (Feng et al., 2001; Feng et al., 2007), suggesting the presence of a hot and wet climate over this part of Australia during interglacial periods. Such climate could also have progressed southward to reach northern New South Wale and cause the reworking of the top horizon of the local tropical regoliths, with the partial dissolution of a fraction of its mineralogy.

6. Conclusion

Kaolinite dating of the duricrusts developed over the Syerston Flemington lateritic deposit demonstrates that these phyllosilicates formed close to the Middle/Late Miocene transition (*ca* 10 Ma combined to a rejuvenated kaolinite age of *ca* 8 Ma), but also during the Pliocene (*ca* 4 Ma) and the Quaternary (*ca* 1 Ma). Such dating results, combined with the crystal-chemistry of the dated kaolinites, demonstrate that:

1) The Syerston regolith formed during two distinct steps: the development of an *in situ* duricrust in the Late/Middle Miocene, then the deposition of a detrital cover followed by its induration between the Pliocene and the Quaternary.

2) This regolith followed an episodic evolution linked to increases in precipitation under a warm and wet climate.

3) The present-day location of this complex laterite, on a local high relief and west of the Great Dividing Range, implies a dissection that caused the retreat of the local scarp of several kilometres in the last 4 Ma. Accordingly, this area of New South Wale should have been characterized, at least punctually, by erosion rates higher than the 6 m/Ma assessed for Central Australia.

4) The Late/Middle Miocene period was favourable for the development of tropical regoliths over southeast Australia. Comparisons with other dating studies of Australian tropical regoliths confirm that some parts of the coastal regions from northwestern to southeastern Australia were also affected during this period by a hot and wet climate. However, further data on the ages of paleosols are needed to specify its extent over the central and coastal parts of the continent during the beginning of Late Miocene.

5) The southeast Australian climate was again favourable to the formation and evolution of tropical regoliths during the Pliocene and likely contributed to the partial rejuvenation of their mineralogy during Quaternary interglacial periods.

These results also question the role of dissolution/recrystallization processes of secondary minerals in the enrichment of metallic elements in regoliths. The presence of at least two generations of kaolinite, from Miocene and Pliocene, in this Sc lateritic deposit (Chassé et al., 2019), confirms that the *in situ* duricrust suffered several episodes of dissolution/recrystallization of secondary minerals. It also demonstrates that part of the *in situ* regolith was accessible to fluid at least until the Pliocene. The leaching of Sc from the upper levels of the duricrust, in parallel to the reworking of its mineralogy, may thus be a dynamic process potentially driven by the impact of regional climatic variations, that will allow the progressive enrichment of the lower horizons of the in situ duricrust. The link between precipitation pulses and the long-term enrichment of critical elements in the tropical regolith should be better constrained through new chronology data on secondary minerals.

Acknowledgments

The authors thank Jervois Mining Ltd for making the drill cores available. The authors thank L. Delbes, M. Guillaumet, the team from ARAMIS (Orsay) and X. François for their help and advice during experiments. We want to thank the reviewers for their detailed review which helped improving the manuscript. The geochemical analytical data were obtained using instrumentation funded by DEST Systemic Infrastructure Grants, ARC LIEF, NCRIS/AuScope, industry partners and Macquarie University. This is contribution 1740 from the ARC Centre of Excellence for Core to Crust Fluid Systems (http://www.ccfs.mq.edu.au) and 1509 in the GEMOC Key Centre (http://www.gemoc.mq.edu.au).

References cited

Aitchison, J. C. & Buckman, S., 2012. Accordion vs. Quantum Tectonics: Insights into Continental Growth Processes from the Paleozoic of Eastern Gondwana. Gondwana Res. 22, 674–680.

Aitken, M.J., 1985. Thermoluminescence dating. Studies in archaeological science. Academic Press, London, 359.

Aleva, G.J.J., and Creutzberg, D., 1994. Laterites: concepts, geology, morphology and chemistry. Wageningen ed., The Netherlands: Internation Soil Reference and Information Center.

Allard, T., Muller, J.P., Dran, J.C., Ménager, M.T., 1994. Radiation-induced paramagnetic defects in natural kaolinite: alpha dosimetry with ion beam irradiation. Phys. and chem. of min., 85-96.

Allard, T., Gautheron, C., Riffel, S.B., Balan, E., Soares, B.F., Pinna-Jamme, R., Derycke, A., Morin G., Bueno, G.T., do Nascimento, N., 2018. Combined dating of goethites and kaolinite from ferruginous duricrusts. Deciphering the Late Neogene erosion history of Central Amazonia. Chem. Geol. 479, 136-150.

Alpers CN, Brimhall GH. 1988. Middle Miocene climatic change in the Atacama Desert, northern Chile: evidence from supergene mineralization at La Escondida. Geol. Soc. Am. Bull. 100, 1640-56.

Ambrosi, J.P., Chen, Y., ESR Dating for lateritic weathering: preliminary approach. Geochem. Earth's Surf. Min. Form., 2nd Intern. Symp., Aix en Provence, France, 19-22.

Anand, R.R., 2001. Evolution, classification and use of ferruginous regolith materials in exploration, Yilgarn Craton. Geochem.: Expl., Env. An. 1, 221-236.

Andrew, A.S., Hensen, B.J., Dunlop, A.C., Agnew, P.D.,1995. Oxygen and Hydrogen Isotope Evidence for the Origin of Platinum-Group Element Mineralization in Alaskan-Type Intrusions at Fifield, Australia. Econ. Geol. 90, 1831-1840.

Angel, B.R., Jones, J.P.E., Hall, P.L., 1974. Electron spin resonance studies of doped synthetic Kaolinite I&II. Clay Min. 10, 247-255.

Balan, E., Allard, T., Boizot, B., Morin, G., Muller, J.P.,1999. Structural Fe^{3+} in natural kaolinite: new insights from electron paramagnetic resonance spectra fitting at X and Q-band frequencies. Clays and Clay Min. 47, 605-616.

Balan, E., Fritsch, E., Allard, T. & Calas, G., 2005. Formation and evolution of lateritic profiles in the middle Amazon basin: Insights from radiation-induced defects in kaolinite. Geoch. and Cosmoch. Acta 69, 2193-2204.

Balan, E., Fritsch, E., Allard, T. & Calas, G., 2007. Inheritance vs. Neoformation of kaolinite during lateritic soil formation: a case study in the middle Amazon Basin. Clays and Clay min. 55 , 253-259.

Beauvais, A., Ruffet, G., Hénocque, O., Colin, F., 2008. Chemical and physical erosion rhythms of the West African Cenozoic morphogenesis: the ^{40}Ar-^{39}Ar of supergene K-Mn oxides. J. of Geophys. Res. 113, F04007.

Beauvais, A., Bonnet, N.J., Chardon, D., Arnaud, N., Jayananda, M., 2016. Very long-term stability of passive margin escarpment constrained by 40Ar/39Ar dating of K-Mn oxides. Geol. 44, 299-302

Bierman, P. R. & Caffee, M., 2002. Cosmogenic exposure and erosion history of Australian bedrock landforms. Geol. Soc. of Am. Bull. 114, 787–803.

Bird, M. I., Chivas, A. R. & McDougall, I., 1990. An isotopic study of surficial alunite in Australia: 2. Potassium–argon geochronology. Chem. Geol. 80, 133–145.

Bonnet, N.J., Beauvais, A., Arnaud, N., Chardon, D., Jayananda, M., 2016. Cenozoic lateritic weathering and erosion history of Peninsular India from 40Ar/39Ar dating of supergene K-Mn oxides. Chem. Geol. 446, 33-53.

Butler, R.F., 1992. Paleomagnetism: Magnetic Domains to Geologic Terranes, Blackwell Scientific Publication.

Cases, J.M., Lietard, O., Yvon, J., Delon, J.F., 1982. Études des propriétés cristallochimiques, morphologiques superficielles de kaolinite désordonnées. Bull. de Min. 105, 439-455.

Carmo I. O., Vasconcelos P. M., 2004. Geochronological evidence for pervasive Miocene weathering, Minas Gerais, Brazil. Earth Surface Processes and Landforms 29, 1303-1320.

Carmo I. O., Vasconcelos P. M., 2006. 40Ar/39Ar geochronology constraints on late Miocene weathering rates in Minas Gerais, Brazil. Earth Planet. Sc. Lett. 241, 80-94.

Chan, R. A., 2009. Evolution of the Girilambone Regolith Landscape, Central-Western New South Wales. Aust. J. of Earth Sci. 56, S106–S123.

Chassé, M., 2017. Geochemical and Crystal-Chemical Processes of Scandium Enrichment from the Mantle to Lateritic Contexts- contribution to the understanding of the processes of critical metals enrichments, Ph.D. thesis, Sorbonne Université.

Chassé, M, Griffin, W.L., O'Reilly S.Y., Calas, G., 2017. Scandium speciation in a world-class lateritic deposit. Geochem. Perspect. Lett. 3, 105-114.

Chassé, M., Griffin, W.L., O'Reilly, S.Y., Calas, G., 2019. Australian Laterites Reveal Mechanisms Governing Scandium Dynamics in the Critical Zone. Geochim. et Cosmochim. Acta 260, 292-310.

Colin, F., Nahon, D., Trescases, J.J., Melfi, A.J., 1990. Lateritic Wreathering of Pyroxenites at Niquelandia, Goias, Brazil: The Supergene Behavior of Nickel. Econ. Geol. 85, 1010-1023.

Cramer, B.S., Toggweiler, J.R., Wright, J.D., Katz, M.E., Miller, K.G., 2013. Ocean overtuning since the Late Cretaceous: Inferences from a new benthic foraminiferal isotope compilation. Paleocean. 24, PA4216.

Dammer, D., Chivas, A. R. & McDougall, I., 1996. Isotopic dating of supergene manganese oxides from Groote Eylandt deposit, Northern Territory, Australia. Econ. Geol. 91, 386–401.

Dammer, D., McDougall, I., Chivas, A.R., 1999. Timing of weathering-induced alteration of manganese deposits in Western Australia; evidence from K/Ar and 40Ar/39Ar dating. Econ. Geol. 94, 87-108

Danišík, M., Evans, N.J., Ramanaidou, E.R., McDonald, B.J., Mayers, C., McInnes, B.I.A., 2013. (U-Th/He) chronology of the Robe River channel iron deposits, Hamersley Province, Western Australia. Chem. Geol. 354, 150-162.

Dequincey, O., Chabaux, F., Clauer, N., Sigmarsson, O., Liewig, N., Leprun, J.C., 2002. Chemical obilizations in laterites: evidence from trace elements and ^{238}U-^{223}U-^{230}Th disequilibria. Geochim. et Cosmochim. Acta 66, 1197-1210.

Dos Santos Albuquerque, M.F., Hollé, A.M.C., Danisik, M., 2020. Episodic weathering in Southwestern Amazonia based on (U-Th)/He dating of Fe and Mn lateritic duricrust, Chem. Geol.553, 119792.

Farmer, V.C., 1974. The layer silicates: The infrared spectra of minerals. The mineralogical society 4, 331-363

Feng Y. X., Vasconcelos P. M., 2001. Quaternary Continental Weathering Geochronology by Laser-Heating 40Ar/39Ar Analysis of Supergene Cryptomelane. Geology 29(7), 635-638.

Feng, Y. X. & Vasconcelos, P. M., 2007. Chronology of Pleistocene weathering process, southeast Queensland, Australia. Earth and Plan. Sci. Lett. 263, 275–287.

Fergusson, C.L., Offler, R., Green, T.J., 2009. Late Neoproterozoic passive margin of East Gondwana; Geochemical constraints from the Analie Inlier, central Queensland, Australia. Precambr. Res. 168, 301-312.

Gaite, J.M., Ermakoff, P. Allard, T., Muller, J.P., 1997. Paramagnetic Fe^{3+}: A sensitive probe for disorder in kaolinite. Clay and clay min. 45, 496-505.

Gallagher, S.J., Smith, A.J., Jonasson, K., Wallas, M.W., Holdgate, G.R., Daniels, J., Taylor, D., 2001. The Miocene palaeoenvironmental and palaeoceanographic evolution of the Gippsland Basin, Southeast Australia: a record of Southern Ocean change. Palaeogeo., Palaeoclim., Palaeoeco. 172, 53-80.

Gallagher, S.J., Greenwood, D.R., J., Taylor, D., Smith, A.J., Wallace, M.W., Holdgate, G.R., 2003. The Pliocene climatic and environmental evolution of southeastern Australia: evidence from the marine and terrestrial realm. Palaeogeo., Palaeoclim., Palaeoeco. 193, 349-382.

Gale, S. J., 1992. Long-term landscape evolution: Australia. Earth Surf. Process. Landforms 17, 323-343.

Greenwood, D.R., Herold, N., Huber, M., Muller, R.D., Seton, M., 2012. Early to middle Miocene monsoon climate in Australia: Reply. Geol. 40, e274.

Guinaseau, D., Fekiacova, Z., Allard, T., Oruhan, J.L., Balan, E., Bouchez, J., 2021. Tropical weathering History Recorded in the Silicon Isotopes of Lateritic Weathering Profiles. Geophy. Res. Lett. 49(19), 1-11.

Heim, J., Vasconcelos, P. M., Shuster, D. L., Farley K. A. & Broadbent, G., 2006. Dating palaeochannel iron ore by (U–Th)/ He analysis of supergene goethite, Hamersley province: Australia. Geol. 34, 173–176.

Heimsath, A.M., Chappel, J., Dietrich, W.E., Kunihiko, N., Finkel, R.C., 2000. Soil production on a retreating escarpment in southeastern Australia. Geol. 28, 787-790.

Heimstath, A. M., Chappell, J., Dietrich, W. E., Nishiizumi, K. & Finkel, R. C., 2001. Late Quaternary erosion in southeastern Australia: a field example using cosmogenic nuclides. Quat. Internat. 83/85, 169–185

Heller, B.M., Riffel, S.B., Allard, T., Morin, G., Roig, J.Y., Couëffé, R., Aertgeerts, G., Derycke, A., Ansart, C., Pinna-Jamme, R., Gautheron, C., 2022. Reading the climate signals hidden in bauxite, Geochimica et Cosmochimica Acta 323, 40-73.

Herold, N., Huber, M., Greenwood, D.R., Müller, R.D., Seton, M., 2011. Early to Middle Miocene monsoon climate in Australia. Geol. 39, 3-6.

Hunt, P.A., Mitchell, P.B., Paton, T.R., 1977. “Laterite profiles” and “lateritic ironstones” on the Hawkesbury sandstone, Australia. Geoder. 19, 105-121.

Korasidis, V.A., Wallace, M.W., Wagstaff, B.E., Hill, R.S., 2019. Terrestrial cooling record through the Eocene-Oligocene transition of Australia. Glob. and Plan. Change 173, 61-72.

Kleeman, J.D., Lovering, J.F., 1967. Uranium distribution in rocks by fission-track registration in lexan plastic. Sci. 156, 512-513.

Li, J.W. & Vasconcelos, P. M., 2002. Cenozoic continental weathering and its implications for the palaeoclimate: evidence from $^{40}Ar/^{39}Ar$ geochronology of supergene K–Mn oxides in Mt Tabor, central Queensland, Australia. Earth and Plan. Sci. Lett. 200, 223–239.

Li J.W., Vasconcelos P. M., Duzgoren-Aydin N., Yan D., Zhang W., Deng X., Zhao X., Zeng Z., Hu M., 2007. Neogene weathering and supergene manganese enrichment in subtropical South China: An 40Ar/39Ar approach and paleoclimatic significance. Earth Planet. Sc. Lett. 256, 389-402

Mao, X., Retallack, G., 2019. Late Miocene drying of central Australia, Pal. Pal. Pal., 514, 292-504.

Mathian, M., Aufort, J., Braun, J.J., Riotte, J., Selo, M., Balan, E., Fritsch, E., Bhattacharya, S., Allard, T., 2019. EPR dating of laterites from Western Ghats (India): a record of Asiatic monsoon strengthening. Gond. Res. 69, 89-105.

Mathian, M., Bueno, G.T., Balan, E., Fritsch, E., Do Nascimento, N.R., Selo, M., Allard, T., 2020. Kaolinite dating from Acrisol and Ferralsol: A new key to understanding the landscape evolution in NW Amazonia (Brazil). Geoder. 370, 114354.

McLaren, S., Wallace, M.W., Gallagher, S.J., Wagstaff, B.E., Tosolini, A.M.P., 2014. The development of a climate- an arid continent with wet fringes. Prins., H&Gordon, I. eds, Invasion Biology and Ecosystem Theory, Cambridge University Press, 256-280.

McGrowan, B.,Li, Q., 1998. Cainozoic climate change and its implication for understanding the Australian regolith. Eggleton R. A. ed. The State of the Regolith. Proceedings of the 2nd Australian Conference on Landscape Evolution and Mineral Exploration, 86 – 103.

Mehra, O.P., Jackson, M.L., 1960. Iron oxide removal from soils and clays by a dithionite-citrate system buffered with sodium bicarbonate. Clays and Clay min. 7, 317-327.

Metzger, C.A., Retallack, G.J., 2010. Paleosol record of Neogene climate change in the Australian outback: Australian Journal of Earth Sciences. An Intern. Geosci.e J. of the Geol.l Soci. of Austr. 57, 871-885.

Miller, H.B.D., Vasconcelos, P.M., Eiler, J.M., Farley, K.A., 2017. A Cenozoic terrestrial paleoclimate record from He dating and stable isotope geochemistry of goethites from Western Australia. Geol.45, 895-898.

Monteiro, H.S., Vasconcelos, P.M., Farley, K.A., Spier, C.A., Mello, C.L., 2014. (U-Th)/He geochronology of goethite and the origin and evolution of cangas. Geochim. et Cosmochim. Acta 131, 267-289.

Morris, R.C., Ramanaidou, E.R., 2007. Genesis of the channel iron deposits (CID) of the Pilbara region, Western Australia. *Austr. J. of Earth Sci.* 54, 733-756.

Nahon, D., 2003. Altérations dans la zone tropicale. Signification à travers les mécanismes anciens et/ou encore actuels. *C. R. Geosci.* 335, 1109-1119.

Nott, J.F., Young, R.W., Idnurm, M., 1991. Sedimentology, weathering, age and geomorphological significance of Tertiary sediments on the far south coast of New South Wales. Austr. J. of Earth Sci. 38, 357-373.

Quilty, P.G., 1994. The background: 144 million years of Australian palaeoclimate and palaeogeography. Hills, R.S. (Ed.), History of the Australian Vegetation: Cretaceous to Recent. Cambridge University Press, Cambridge, 14-43.

Pidgeon, R. T., Brander, T. & Lippolt, H. J., 2004. Late Miocene (U– Th)/He ages of ferruginous nodules from lateritic duricrust, Darling Range, Western Australia. Austr. J. of Earth Sci. 51, 901–909.

Pickett, J. W., 2003. Stratigraphic relationships of laterite at Little Bay, near Maroubra, New South Wales. Austr. J. of Earth Sci. 50, 63-68.

Pillans, B., 2004. Geochronology of the Australian regolith. Geochronol., CRC LEME 2004, 1-12.

Putzolu, F., Abad, I., Balassone, G., Boni, M., Cappelletti, P., Graziano, S.F., Maczurad, M., Mondillo, N., Najorka, J., Santoro, L., 2020. Parent rock and climatic evolution control on the genesis of Ni-bearing clays in Ni-Co laterites: New inferences from the Wingellina deposit (Western Australia). Ore Geol. Rev. 120, 103431.

Ramanaidou, E.R., Morris, R.C., Horwitz, R.C., 2003. Channel iron deposits of the Hamersley Province, Western Australia. Austr. J. of Earth Sci. 50, 669-690.

Ramanaidou, E.R., Wells, M.A., Morris, R., Duclaux, G., Evans, K., Danisik, M., 2017. Channel iron deposits of the Pilbara. Australian Ore Deposits, ed. Philips, G.N., 375-380.

Retallack, G.J. (2010) Lateritization and Bauxitization Events. Econ. Geol. 105, 655-667.

Riffel, S.B., Vasconcelos, P.M., Carmo, I.O., Farley, K.A., 2015. Combined 40Ar/39Ar and (U-Th)/He geochronological constraints on long-term landscape evolution of the Second Parana Plateau and its ruiniform surface features, Parana, Brazil. Geomorphol. 233, 52-63.

Russel, J.D., Fraser, A.R., 1994. Infrared methods: Clay mineralogy: Spectroscopic and Chemical Determinative methods. London: ed. Chapman et al., 11-67

Sakoda, A., Ishimori, Y., Yamaoka, K., 2011. A comprehensive review of radon emanation measurements for mineral, rock, soil, mail tailing and fly ash. Appl. Rad. and Isot. 69, 1422-1435

Schmidt, P.W., Williams, G.E., 2017. Paleomagnetic age of ferruginous weathering beneath the Hamersley Surface, Pilbara, Western Australia, and the Cenozoic apparent polar wander path. Austr. J. of Earth Sci. 64, 239-249.

Sélo, M., 1983. La fission nucléaire et sa signification en géochronomogie, paléothermométrie et géochimie. Applications à l'étude particulière des basalts océaniques. Ph.D. thesis, Université Paris VI.

Shuster, D.L., Vasconcelos, P.M., Heim, J.A., Farley, K.A., 2005. Weatehring geochronology by (U-Th)/He dating of goethite. Geochim. et Cosmochim. Acta 69, 659-673.

Tardy, Y., 1993. Pétrologie des latérites et des sols tropicaux. Ed. Masson, 401-404.

Travouillon, K.J., Legendre, S., Archer, M., and Hand, S.J., 2009. Palaeoecological analyses of Riversleigh's Oligo-Miocene sites: Implications for Oligo-Miocene climate change in Australia. Palaeogeo., Palaeoclim., Palaeoeco. 276, 24–37

Vasconcelos P. M., Rene P.R., Brimhall G.H., and Becker T.A. (1994). Direct dating of weathering phenomena by 40Ar/39Ar and K-Ar analysis of supergene K-Mn oxides. Geochim. Cosmochim. Acta 58, 1635-1665

Vasconcelos, P.M., 1998. Geochronology of weathering in the Mount Isa and Charters Towers regions, northern Queensland. CRC LEME Open-File Report 139 (2002).

Vasconcelos, P.M., 1999. K-Ar AND $^{40}Ar/^{39}Ar$ Geochronology of weathering processes. Annu. Rev. of Earth and Plan. Sci. 27, 183-229.

Vasconcelos, P.M., Conroy, M., 2003. Geochronology of weathering and landscape evolution Dugald River valley, NW Queensland, Australia. Geochim. et Cosmochim. Acta 67, 29132930.

Vasconcelos, P.M., Knesel, K.M., Cohen, B.E., Heim, J.A., 2008. Geochronology of the Australian Cenozoic: a history of tectonic and igneous activity, weathering, erosion and sedimentation. Austr. J.l of Earth Sci. 55, 865-914.

Vasconcelos, P.M., Heim, J.A., Farley, K.A., Monteiro, H., Waltenberg, K., 2013. 40Ar/39Ar and (U-Th)/He-4He/3He geochronology of landscape evolution and channel iron deposit genesis at Lynn Peak, Western Australia. Geochim. et Cosmochim. Acta 117, 283-312.

Vasconcelos, P.M, Farley, K.A., Stone, J., Piacentini, T., Fifield, L.K., 2019. Stranded landscapes in the humid tropics: Earth's oldest land surfaces. Earth and Plan. Sci. Lett. 519, 152-164.

Wells, M.A., Danisik, M., McInnes, B.I.A., Morris, P.A., 2019. (U-Th)/He dating of ferruginous duricrust: Insight into laterite formation at Boddington, WA. Chem. Geol. 522, 148-161

Yongue-Fouateu, R., Yemefack, M., Wouatong, A.S.L., Ndjigui, P.D., Bilong, P., 2009. Contrasted mineralogical composition of the laterite cover on serpentinites og Nkamouna-Kong, southeast Cameroon. Clay Min. 44, 221-237.

Zachos, J., Pagani, M, Sloan, L., Thomas, E., Billups, K., 2001. Trends, Rhythms, and Aberrations in Global Climate 65 Ma to Present. Sci. 292, 686-693.

Ziegler, J.F., Ziegler, M.D., Biersack, J.P., 2010. *SRIM-The Stopping and Range of Ions in Matter*.

Figure Captions

Fig. 1: Topographic map of Australia (ASTER GDEM 2019: ASTER GDEM is a product of METI and NASA). Green spots are the locations of previous secondary minerals dating applied to Australian tropical regoliths (Bird et al., 1990; Dammer et al., 1996; Dammer et al., 1999; Li and Vasconcelos, 2002; Vasconcelos and Conroy, 2003; Pidgeon et al., 2004; Heim et al., 2006; Feng and Vasconcelos, 2007; Vasconcelos et al., 2008 and references therein; Vasconcelos et al., 2013; Danisik et al. 2013; Miller et al., 2017 and references therein; Wells et al., 2019). The location of figure 2A (red square) and of the Syerston-Flemington deposit area (orange spot) are also displayed on the topographic map.

Fig. 2: A: Regional topographic map centred around the Syerston-Flemington deposit (ASTER GDEM 2019: ASTER GDEM is a product of METI and NASA). B: Topographic profile of a transect perpendicular to the dissected scarp hosting the Syerston tropical regolith. C: Geological map of the Tout-complex, forming the parent rock of the studied regolith, with the location of the studied profile developed over the local clinopyroxenite (drilling area).

Fig. 3: Regolith profile structure, sample location, mineralogy of the main horizons of this profile and of the four bulk samples selected for dating (after Chassé et al., 2019). All the methods used for the semi-quantification of mineral phases from the samples X-ray diffraction patterns and the XRD patterns themselves are described in Chassé et al. (2019).

Fig. 4: EPR spectra of a reference kaolinite (GB1 kaolinite, see Cases et al., 1982) and of the insitu1 sample. The EPR spectra of kaolinite-rich samples are divided into two domains: the g=4 area hosting the signal of Fe^{3+} ions substituted to Al^{3+} within the kaolinite structure, and the g=2 domain hosting the signal of Radiation Induced Defects (RID) used as a geochronometer for the EPR dating of phyllosilicates. The first domain is commonly used as a probe to estimate the kaolinite degree of crystalline disorder, as the $Fe_{(I)}$ signal increases in parallel to the disorder of kaolinite (e.g. the GB1 kaolinite is well ordered while the insitu1 sample is poorly ordered). A zoom for the g=2 spectral region is also provided.

Fig. 5: A: Insitu2 sample general petrographic arrangement with kaolinite plates dispersed within an unorganized Fe oxide-rich matrix. This sample has a similar organization to that of insitu1 sample except for: 1) larger kaolinite plates; 2) some kaolinite plates organized into structures reminding vermicular shapes; 3) greater porosity. B: General petrographic arrangement of detrit1 sample and zoom for kaolinite vermicules. The kaolinite formed more or less rounded geometric plates or small vermicules with a low preservation (fractures). Some traces of kaolinite overgrowths are detected on some fractured vermicules. C: General petrographic arrangement of detrit2 sample and zoom for observed kaolinite vermicules. This sample displays either vermicules with a low preservation grade (fractures) and larger vermicules with a good preservation grades. A large part of the kaolinite is also present as plates within the matrix. D: FTIR spectra of the studied samples. The detrit1 sample is particularly rich in gibbsite and its kaolinite was more disordered than the 3 others. E: EPR spectra of the detrit1 and insitu1 sample, the latter is representative of the EPR spectra of the insitu2 and detrit2 samples. The detrit1 sample displays the characteristic spectrum of highly disordered kaolinite while the three others are typical of disordered kaolinite.

Fig. 6: Conceptual diagram of duricrust formation and distribution of kaolinite crystallization ages along the regolith profile. Three main discrete periods of weathering driven by tropical climate forcing are revealed during Miocene, Pliocene and Quaternary.

Fig.7: Time chart presenting the main tropical weathering periods from Miocene to Present in southeast Australia along with kaolinite ages from the present study (P.W.: Pliocene Warming; M.W.: Miocene Warming; NSW: New South Wale; MMCO: Mid Miocene Climatic Optimum). Only the Quaternary weathering period remains unrelated.

Fig. 8: Comparison of EPR dating kaolinite ages from this study (insitu1 the red dash line, detrit1 the orange dash line, insitu2 the green dash line and detrit2 the blue dash line with their error range displays in transparency) with histograms combining results from Ar/Ar, K/Ar and (U-Th)/He dating of secondary minerals from tropical weathering profiles located in Southwest, Northwest and Northeast Australia and the main event of evolution of global climate (Zachos et al., 2001; Cramer et al., 2013). Each of these regions, and particularly the Northwest and Northeast Australia, was impacted by a tropical climate during the Mid-Miocene and also in the beginning of the Late Miocene. The histograms were made combining the results of Bird et al. (1990), Dammer et al. (1996), Dammer et al. (1999), Li and Vasconcelos (2002), Vasconcelos and Conroy (2003), Pidgeon et al. (2004), Heim et al. (2006), Feng and Vasconcelos, (2007), Vasconcelos et al. (2008) and references therein; Vasconcelos et al. (2013), Danisik et al. (2013), Miller et al. (2017) and references therein; Wells et al. (2019).

Table 1: Characteristics and calculated ages of the kaolinite samples.

Sample	Depth (m)	Kaolinite Proportion (%)	Amplitude RID (U.A.)	Paleodose (kGy)	[U] (ppm)	[Th] (ppm)	K (%)	U in U-Bearers Mineral (%)	U matrice (%)	[Th] /[U]	Dose rate uncorrected (Gy/ka)	Dose rate corrected (Gy/ka)	Age corrected (Ma)
detrit2	***3***	***19***	2.72	10.6±2.87	1.42	10.92	0	68.15	31.85	7.69	13.12±0.87	10.26±0.68	1.03±0.28
detrit1	***6.5***	***11***	6.33	68.59±22.93	1.35	8.67	0	68.15	31.85	6.42	11.09±0.76	8.4±0.57	8.17±2.78
insitu2	***16***	***23***	1.358	8.12±1.84	0.69	1.34	0	10.05	89.95	3.43	2.26±0.17	2.12±0.16	3.83±0.91
insitu1	***16.4***	***33***	1.244	15.55±3.11	0.33	0.8	0	10.05	89.95	2.42	1.64±0.16	1.53±0.15	10.09±2.26

Figure 1:

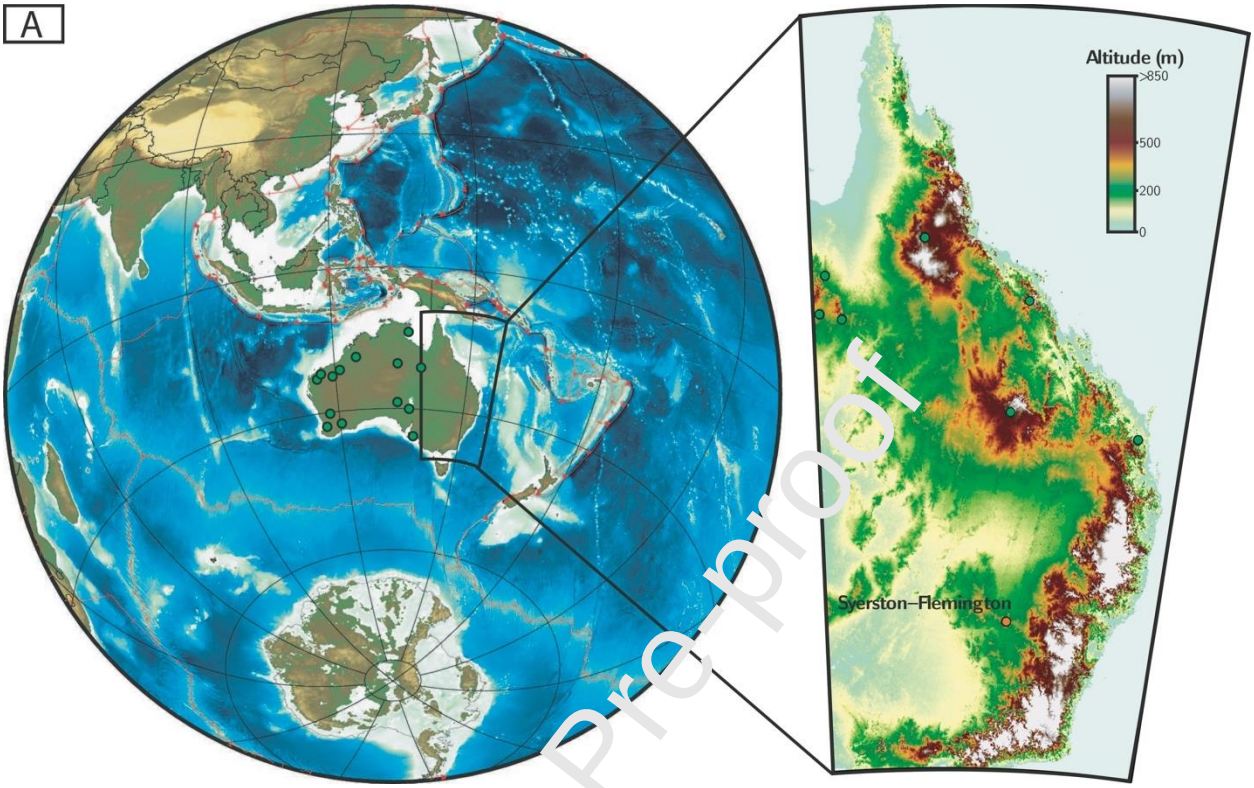

Figure 2:

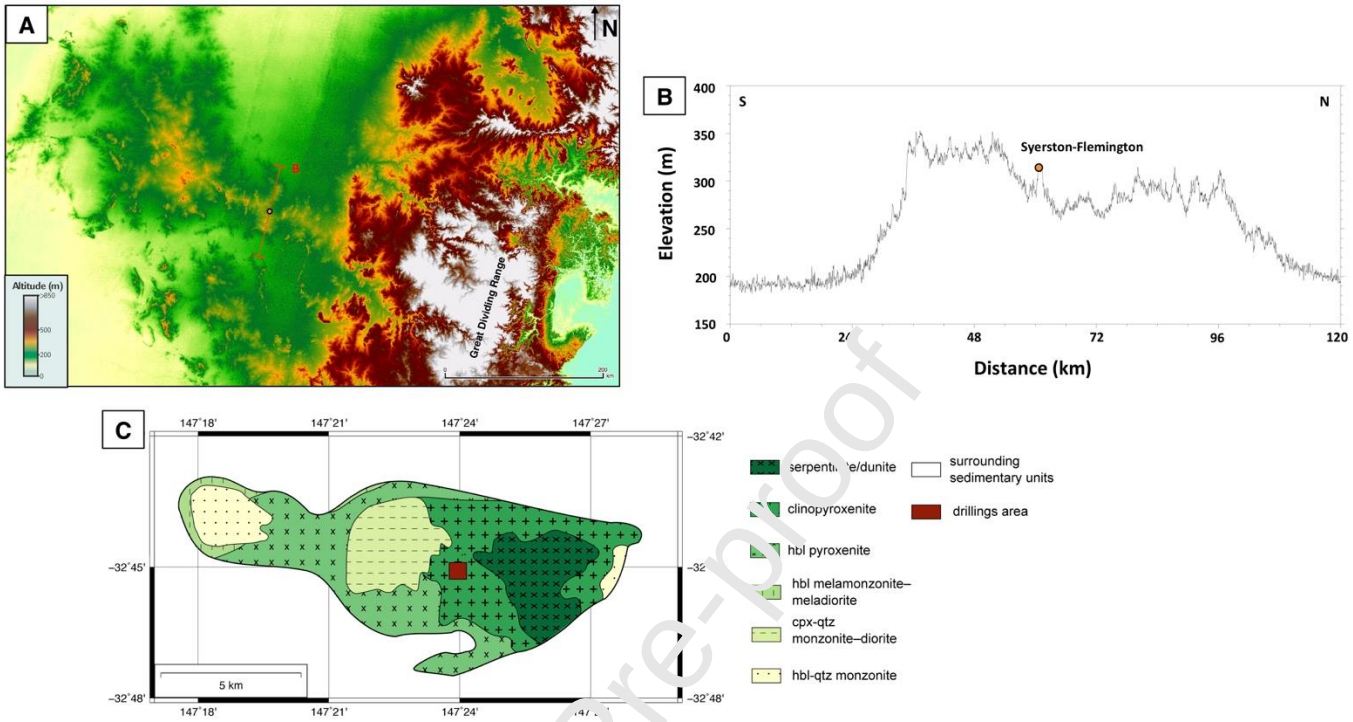

Figure 3:

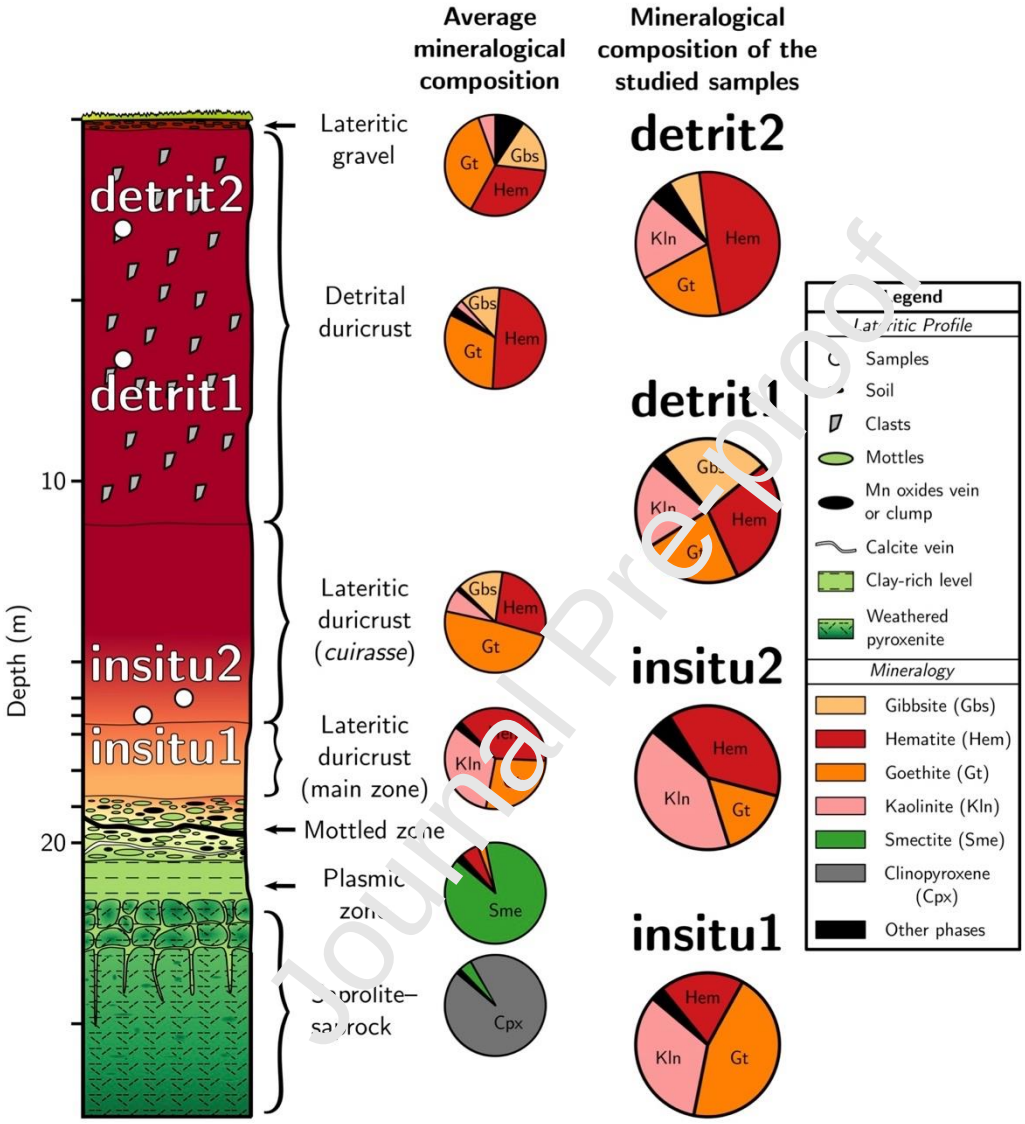

Figure 4:

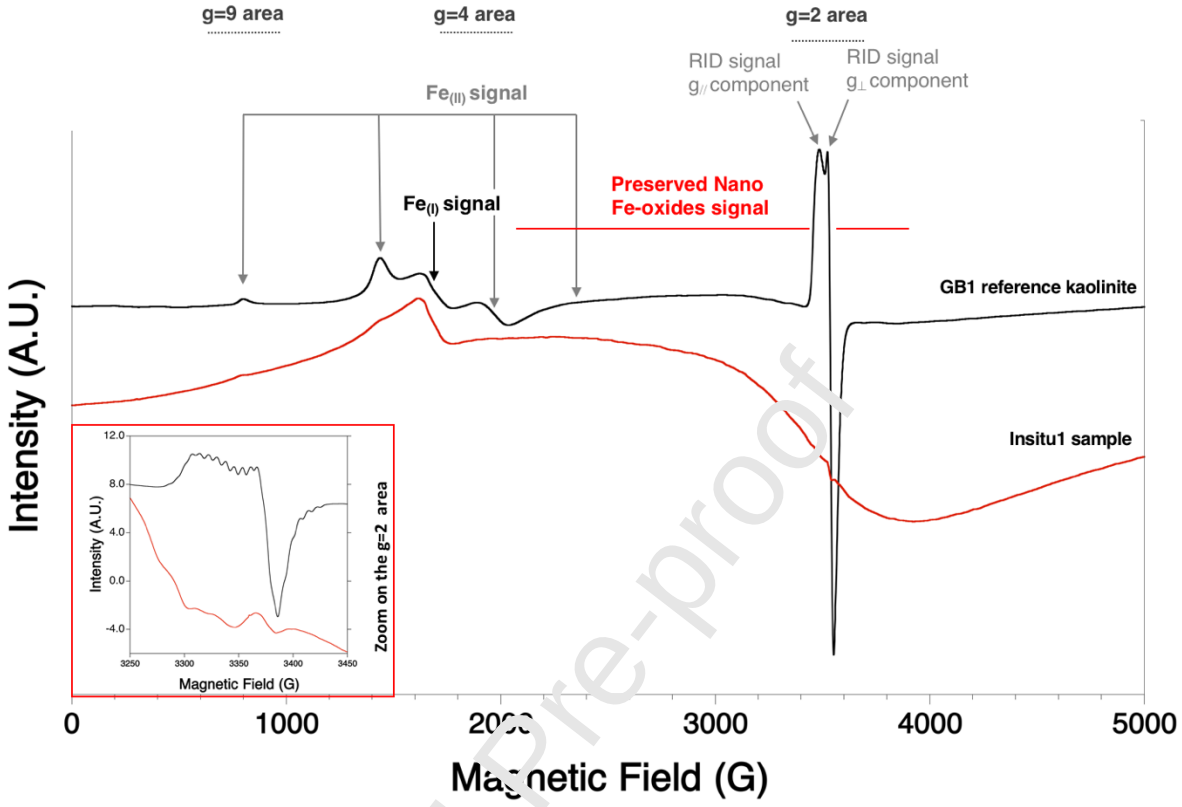

Figure 5:

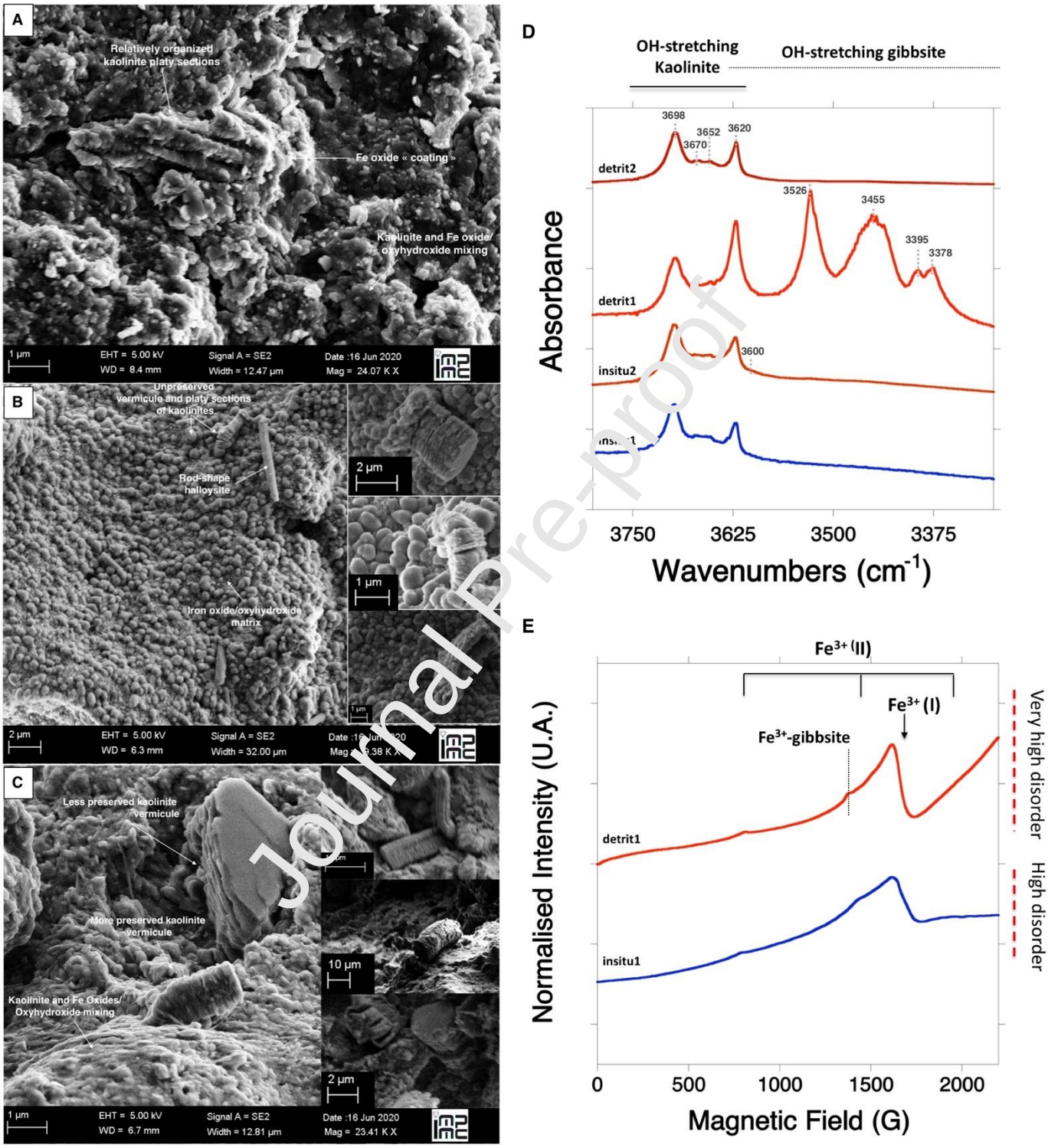

Figure 6:

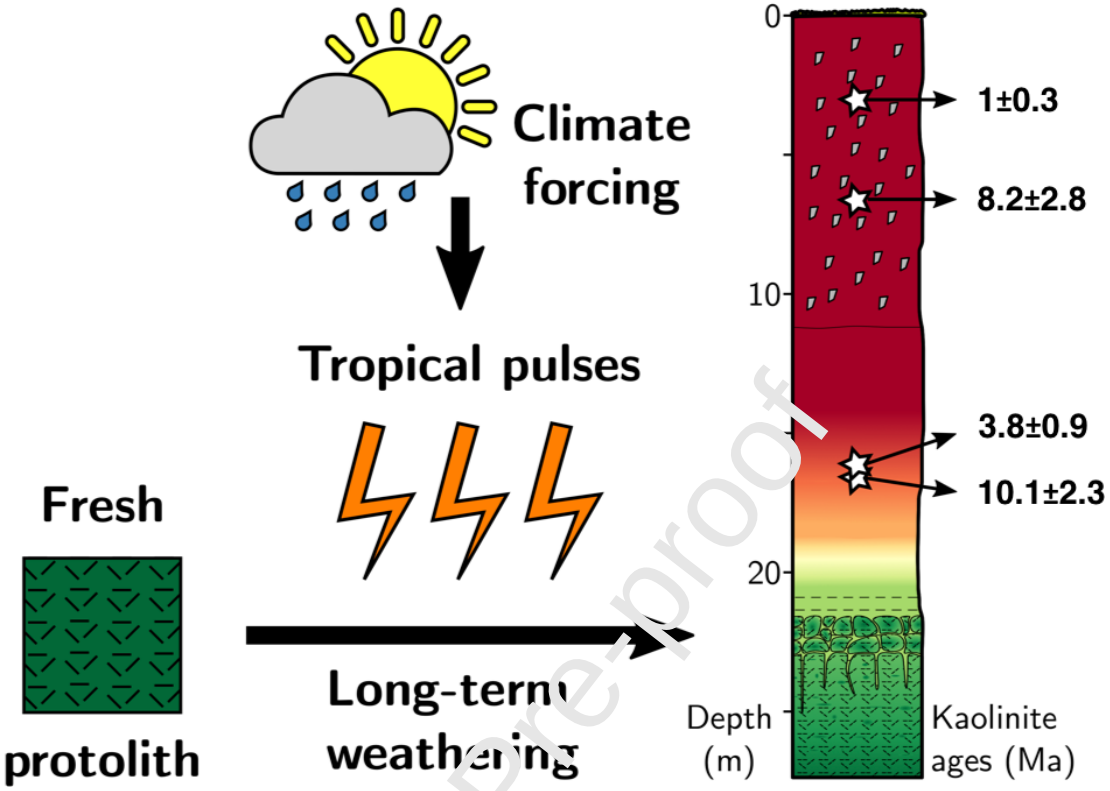

Figure 7:

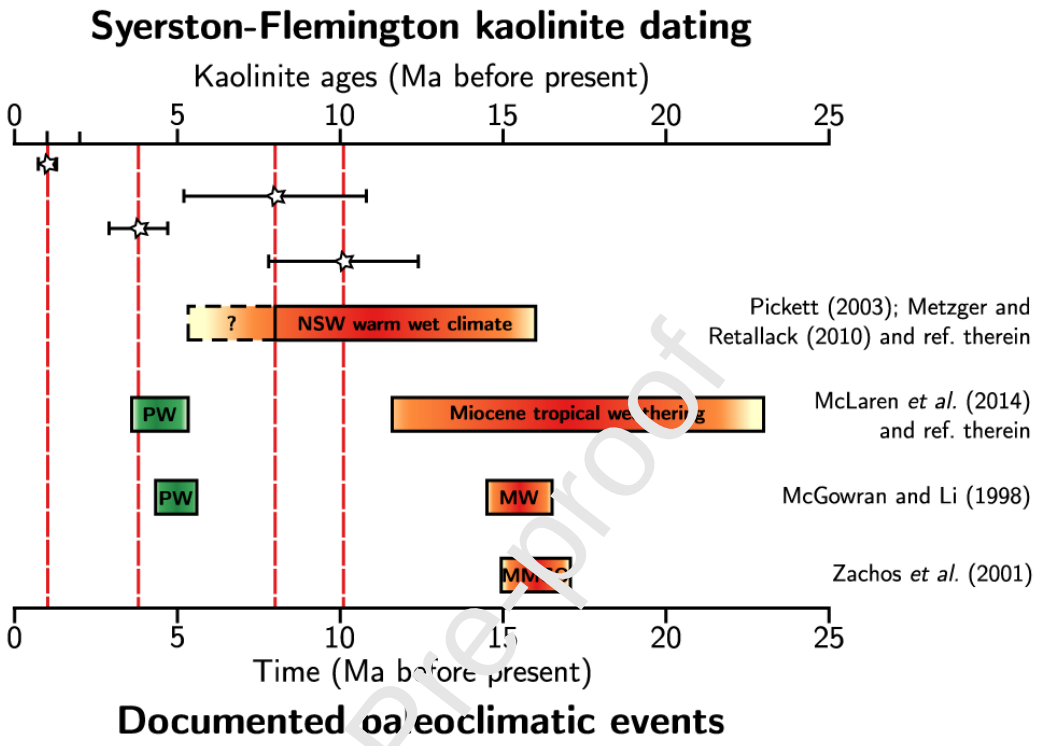

Figure 8:

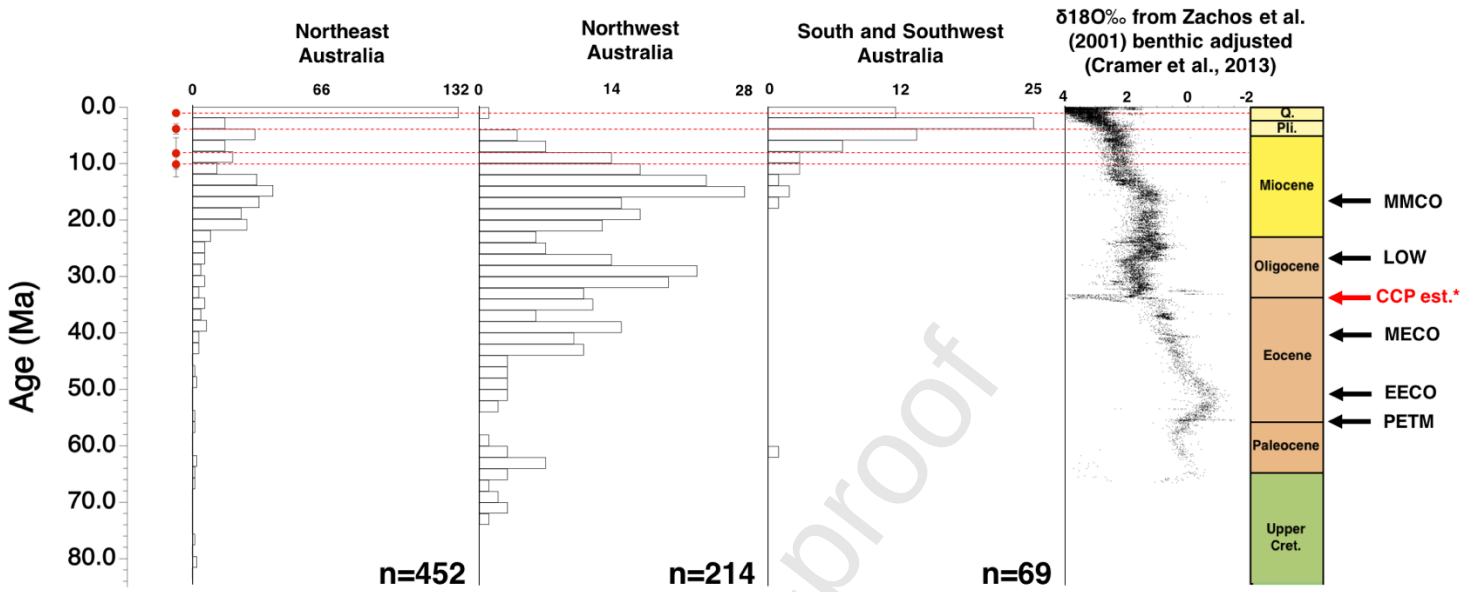

Declaration of interests

☒ The authors declare that they have no known competing financial interests or personal relationships that could have appeared to influence the work reported in this paper.

☐The authors declare the following financial interests/personal relationships which may be considered as potential competing interests:

Highlights :

- Chronological constraints on regoliths formation are poor in southeastern Australia
- This study is focused on a complex tropical regolith from southeast Australia
- Kaolinites from the local insitu and detrital duricrusts were dated using EPR dating
- Miocene (10.1 and 8 Ma), Pliocene (3.8) and Quaternary generations were observed
- It evidenced the presence of a tropical coastal line in the Mid and Late Miocene